Zero Voltage Soft-Commutation PWM DC–DC Converter with Saturable Reactor Switch-Cascaded Diode Rectifier

Junming Sun, Satoshi Hamada, Junji Yoshitsugu, Bin Guo, and Mutsuo Nakaoka, *Member, IEEE*

***Abstract*— An improved single-ended push–pull (SEPP) half-bridge type zero-voltage soft-switching pulse width modulation (ZVS-PWM) DC–DC power converter is presented in this paper, which makes use of a saturable reactor-assisted lossless capacitor type zero voltage soft-switching method. The SEPP power converter with a high-frequency forward and flyback hybrid transformer link has some advantages such as lowered switching and conduction losses, soft-switching transition operation over a wide load range, constant frequency PWM regulation and minimized Electro Magnetic Interference (EMI) as well as Radio Frequency Interference (RFI) noises. Its operating principle is illustrated and its periodic steady-state circuit analysis are implemented. In order to demonstrate the remarkable effectiveness of this converter characteristics, feasible experiments are actually implemented with a 150-W–200-kHz prototype of high-frequency link ZVS-PWM DC–DC converter using power MOSFET's with ultrafast soft-recovery diode.**

***Index Terms*— Asymmetrical PWM, DC–DC converter, forward and flyback hybrid transformer mode, high-frequency isolated link, lossless capacitive snubbers, low voltage and large current applications, saturable reactor switch, zero-voltage soft-switching, single-ended push–pull.**

I. Introduction

IN GENERAL, in order to increase the power density of the switched-mode power supply circuits and to improve their operating performance, it is dispensable to raise the switching operating frequency of the power conversion supplies to reduce physical size and weight of their reactive circuit components incorporated into the converters. A variety of zero-voltage and zero-current soft-switching PWM converter circuit topologies using new power semiconductor devices and modules such as trench-type power MOSFET's, Static Induction Transistors (SIT's), Bipolar mode SIT's (B-SIT's), and Insulated Gate Bipolar Power Transistors (IGBT's). Their topologies are able to reduce their switching losses, their voltage and current surges related to their parasitic parameters and to lower the saturation voltage of power devices to allow high-frequency operation together with their control schemes, have been proposed so far. These soft-switched PWM converters basically provide a number of inherent salient advantages, such as low switching losses, lowered EMI, constant frequency power regulation operation and simple control scheme [1].

However, these kinds of soft-switching schemes converter circuits topologies for are difficult to achieve complete zero-voltage switching in wide operating load ranges from light to heavy loads. Furthermore, current and/or voltage peak stresses applied to active and passive circuit components are still high as compared with those of conventional hard-switching PWM converters. In addition to this, resonant-mode soft-switching converters includes load dependent characteristics in soft-switching operation.

In recent years, several types of soft-switching PWM DC–DC power converters employing the saturable reactor-assisted (SRA) lossless snubber type quasi-resonant soft-switching techniques have been originally introduced by many researchers and authors. It is proved from a practical point of view that some types of power converters can operate under the conditions of soft-switching operation over relatively wide load range without substantial increase in total conduction losses as well as voltage and current stresses.

It is noted that this type of converter developed by the authors [2]–[8] has inherent excellent characteristics of both hard-switching PWM and quasi-resonant-mode soft-switching converters.

In this paper, a newly developed asymmetrical PWM SEPP converter with forward and flyback-operated high-frequency transformer link using a simple saturable reactor-assisted lossless capacitor snubber type (SRA) soft-switching technique is presented. The operation principle of this converter and its steady-state periodic circuit analysis are described herein. Its voltage conversion ratio, voltage and current peak stresses applied to active and passive circuit components in this converter are also evaluated and discussed from a theoretical viewpoint. In order to demonstrate the effectiveness based on the characteistic performances, feasible experiments are actually carried out in terms of using a 200-kHz–150-W prototype of soft-switching power converter breadboard that incorporates the latest power MOSFET modules with ultrafast soft recovery diode and their driver IC modules.

II. Circuit Description and Operating Analysis

A. Circuit Configuration

Fig. 1 shows a schematic circuit system and its typical steady-state voltage and current waveforms of the proposed SRA lossless capacitor snubber type soft-switching asymmet-

Manuscript received October 9, 1996; revised February 6, 1997 and April 9, 1997. This paper was recommended by Associate Editor L. Martínez-Salamero.

The authors are with the Graduate School of Engineering and Science, Yamaguchi University, 2557 Tokiwa-dai, Ube, Yamaguchi, 755 Japan.

Publisher Item Identifier S 1057-7122(98)02113-8.

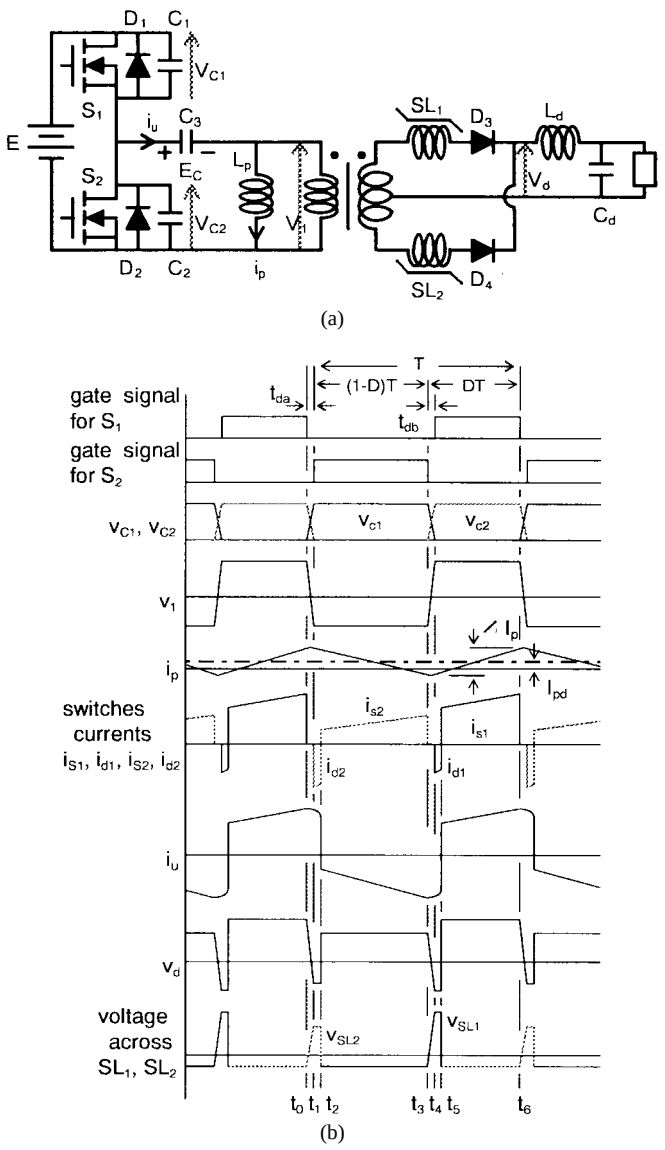

Fig. 1. SRA soft-switching PWM converter with lossless capacitive snubbers and its typical operating waveforms.

rical PWM forward–flyback hybrid transformer link DC–DC power converter operating at ZVT switching mode. The active power switches S_1 and S_2 are driven alternately with short blanking intervals t_{da} and t_{db}. SL_1 and SL_2 are piecewise-linear inductance-based saturable reactors composed of small amorphous cores with ritzwire windings which act as flux-regulated magnetic switches with small residual inductance and have a great deal of contribution to achieve zero voltage soft-switching transition for the active power switches S_1, S_2 and the passive diode switches D_3, D_4 as the rectifier. Note that these magnetic switches SL_1, SL_2 in series with diodes act as active power switches. The DC output voltage or power of this converter is smoothly regulated by controlling the duty ratio D as a control variable under a condition of a constant inverter frequency.

B. Operation Principle and Steady-State Analysis

The respective equivalent circuit corresponding to each mode during one cycle converter operation is illustrated in Fig. 2.

Just before the time t_0, the active switch S_1 and the diode D_3 are still conducting. The nonlinear reactor SL_1 is saturated, whereas SL_2 is unsaturated.

1) Mode 1 ($t_0 \le t \le t_1$): The switch S_1 is turned off at the time t_0. The equivalent circuit during this interval is shown in Fig. 2(a). The current through the switch S_1 is transferred to the capacitors C_1 and C_2 as a lossless capacitive snubbers. The voltage $v_{c1}(t)$ across the capacitor C_1 in high-side bridge arm and the inductor current $i_p(t)$ of additional inductor L_p in parallel with a transformer are estimated by

$$v_{c1}(t) = Z_n\{I_0 + i_p(t_0)\}\sin\omega_n t + (E - E_c)(1 - \cos\omega_n t) \tag{1a}$$

$$i_p(t) = -I_0 + \{I_0 + i_p(t_0)\}\cos\omega_n t + \frac{E - E_c}{Z_n}\sin\omega_n t \tag{1b}$$

where

$$\omega_n = \frac{1}{\sqrt{2L_pC}}, \quad Z_n = \sqrt{\frac{L_p}{2C}}, \quad C_1 = C_2.$$

As a result, the voltage $v_{c1}(t)$ increases. As the voltage $v_{c1}(t)$ reaches $E - E_c$ the high-frequency isolated transformer link voltage $v_1(t)$ in the intermediate power-stage changes from positive to negative. Because SL_2 is still unsaturated, the rectifier diode D_3 continues to conduct. When the voltage $v_{c1}(t)$ reaches E, the body diode D_2 turns on. The switching transition interval $t_{\gamma a}$ is derived from (1a) as

$$t_{\gamma a} = \frac{1}{\omega_n}(\psi_1 + \psi_2) \tag{1c}$$

where

$$\psi_1 = \sin^{-1}\frac{E_c}{\sqrt{[Z_n\{i_p(t_0) + I_0\}]^2 + (E - E_c)^2}}$$

$$\psi_2 = \tan^{-1}\frac{E - E_c}{Z_n\{i_p(t_0) + I_0\}}$$

2) Mode 2 ($t_1 \le t \le t_2$): The body diode D_2 conducts when $v_{c1}(t)$ reaches E. The transformer-link voltage $v_1(t)$ becomes E_c. The magnetic core flux for SL_2 comes to increase in accordance with the voltage integral effect. The load current referred to the primary-side of the high-frequency transformer flows through the body diode D_2 and the energy storage capacitor C_3.

The equivalent circuit during this interval is illustrated in Fig. 2(b). The state variables $v_{c1}(t)$ and $i_p(t)$ are estimated by

$$v_{c1}(t) = E \tag{2a}$$

$$i_p(t) = i_p(t_1) - \frac{E_c}{L_p}(t - t_1) \tag{2b}$$

where L_p is replaced by the equivalent magnetizing inductance of the high-frequency transformer. This interval ends when SL_2 reaches a saturation level.

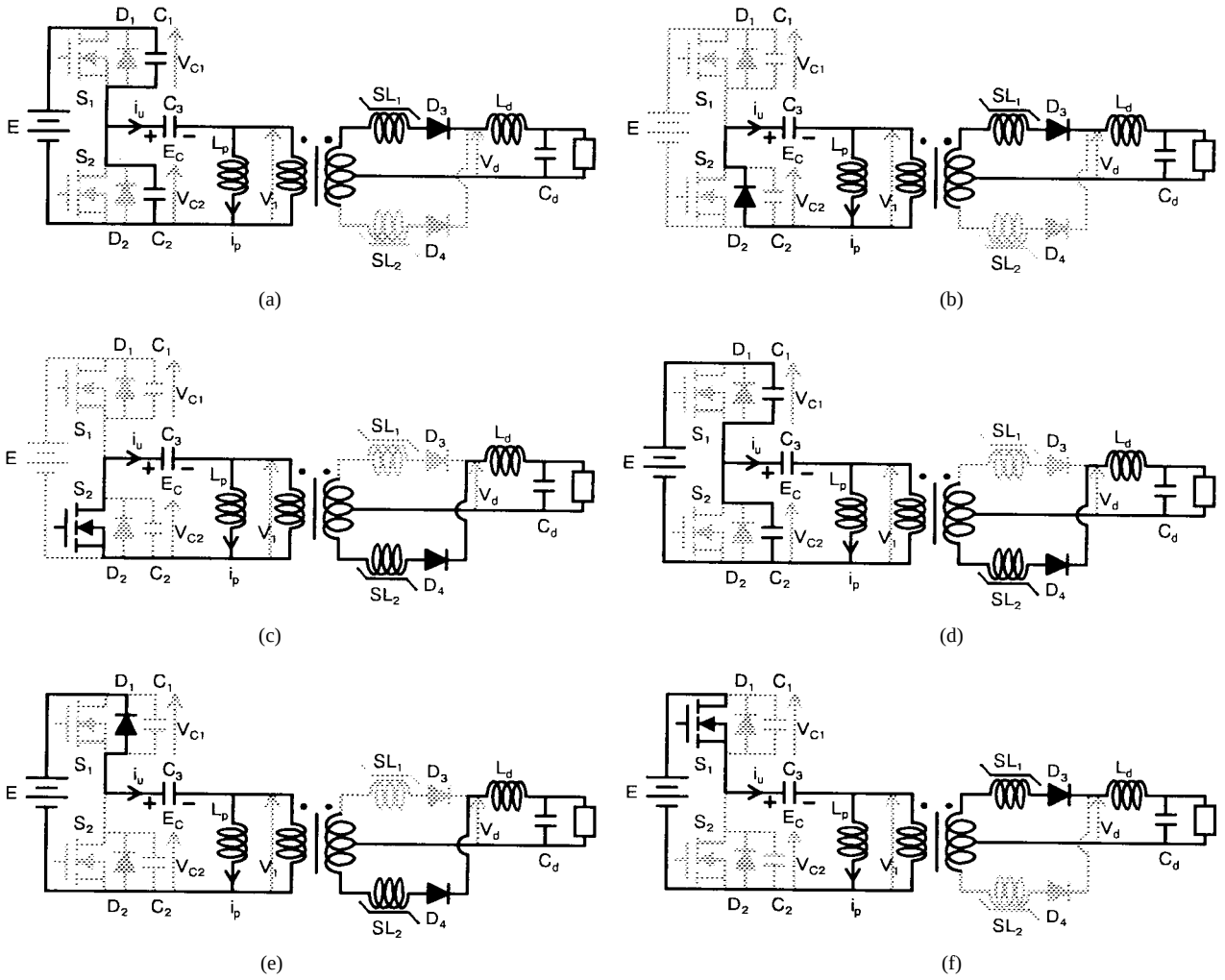

Fig. 2. Topological circuits during one operation cycle.

3) Mode 3 ($t_3 \le t \le t_3$): As soon as the saturable reactor SL_2 reaches a saturation level, the rectifier diode D_4 starts to conduct. And the rectifier diode D_3 is turned off and SL_1 becomes unsaturated. Thus, the ideal transformer current $i_1(t)$ in its primary side changes instantaneously from I_0 to $-I_0$.

The injected current $i_u(t)$ of the transformer is given as

$$i_u(t) = i_p(t) - I_0. \tag{3a}$$

The switch S_2 starts to conduct when the current $i_u(t)$ becomes $i_u(t) < 0$. The state variables $v_{c1}(t)$ and $i_p(t)$ are estimated by

$$v_{c1}(t) = E \tag{3b}$$

$$i_p(t) = i_p(t_2) - \frac{E_c}{L_p}(t - t_2). \tag{3c}$$

4) Mode 4 ($t_3 \le t \le t_4$): The switch S_2 is turned off at time t_3, which depends on the duty ratio D as a control variable. The current through the switch S_2 is transferred to the snubber capacitors C_1 and C_2. The equivalent circuit during this interval is shown in Fig. 2(d). The voltage $v_{c1}(t)$ decreases. The state variables $v_{c1}(t)$ and $i_p(t)$ are expressed as

$$v_{c1}(t) = (E - E_c) + E_c \cos\omega_n(t - t_3) - Z_n\{I_0 - i_p(t_3)\}\sin\omega_n(t - t_3) \tag{4a}$$

$$i_p(t) = I_0 - \frac{E_c}{Z_n}\sin\omega_n(t - t_3) - \{I_0 - i_p(t_3)\}\cos\omega_n(t - t_3). \tag{4b}$$

As the voltage $v_{c1}(t)$ becomes $(E - Ec)$, the transformer-link voltage $v_1(t)$ changes from negative to positive. In this case, the rectifier diode D_4 continues to conduct. Because the saturable reactor SL_1 is unsaturated. The body diode D_1 turns on when the voltage $v_{c1}(t)$ is lowered to zero. The switching transition interval $t_{\gamma b}$ is derived from (4a) as

$$t_{\gamma b} = \frac{1}{\omega_n(\psi_3 + \psi_4)} \tag{4c}$$

where

$$\psi_3 = \sin^{-1}\frac{E - E_c}{\sqrt{[Z_n\{I_0 - i_p(t_3)\}]^2 + E_c^2}}$$

$$\psi_4 = \tan^{-1}\frac{E_c}{Z_n\{I_0 - i_p(t_3)\}}$$

5) Mode 5 ($t_4 \le t \le t_5$): The load current reflected to the transformer primary side flows through the high-frequency link capacitor C_3 and the body diode D_1. The state variables $v_{c1}(t)$ and $i_p(t)$ are given by

$$v_{c1}(t) = 0 \tag{5a}$$

$$i_p(t) = i_p(t_4) + \frac{E - E_c}{L_p}(t - t_4). \tag{5b}$$

In this case, the magnetic core flux $\Phi$for SL_1 is increased up to Φ_1.

6) Mode 6 ($t_5 \le t \le t_6$): As soon as the saturable reactor SL_1 reaches a saturation level, the rectifier diode D_3 starts to conduct. The state variables: $v_{cl}(t)$ and $i_p(t)$ are expressed as

$$v_{c1}(t) = 0 \tag{6a}$$

$$i_p(t) = i_p(t_5) + \frac{E - E_c}{L_p}(t - t_5). \tag{6b}$$

The ideal transformer current $i_1(t)$ changes from $-I_0$ to I_0 instantaneously. As a result, the bridge current $i_u(t)$ is given as

$$i_u(t) = i_p(t) + I_0. \tag{6c}$$

The active power switch S_1 starts to conduct under zero-voltage condition when the bridge current $i_u(t)$ becomes >0. The one cycle during the inverter switching interval ends at time t_6.

C. Steady-Steady Performance Evaluations

Assuming that ψ_1, ψ_2, ψ_3, and $\psi_4 \ll \pi/2$, the switching-mode transition intervals $t_{\gamma a}$ and $t_{\gamma b}$ are given by

$$t_{\gamma a} = \frac{2CE}{I_0 + i_p(t_0)} \tag{7}$$

$$t_{\gamma b} = \frac{2CE}{I_0 - i_p(t)3e)}. \tag{8}$$

The volt-seconds for the high-frequency transformer during one cycle period T is expressed as

$$\int_0^T v_1(t)\, dt = 0. \tag{9}$$

Assuming that the transformer voltage $v_1(t)$ is nearly square waveform because $t_{\gamma a}$ and $t_{\gamma b}$ are quite short, capacitor voltage E_c is approximately derived from (9) as

$$(E - E_c)DT - E_c(1 - D)T = 0 \tag{10}$$

$$E_c = DE. \tag{11}$$

The average current flowing through the energy storage capacitor during one cycle T has to be

$$\int_0^T i_u(t)\, dt = 0 \tag{12}$$

Substituting (3a) and (6c) into (12),

$$\int_0^{DT} \{i_p(t) + I_0\}\, dt + \int_{DT}^T \{i_p(t) - I_0\}\, dt = 0. \tag{13}$$

In this case, the commutation inductor current $i_p(t)$ is expressed as

$$i_p(t) = I_{pd} + i_{pa}(t) \tag{14}$$

where I_{pd} is the DC component of $i_p(t)$ and $i_{pa}(t)$ is the AC component of $i_p(t)$.

Since $\int_0^T i_{pa}(t) = 0, I_{pd}$ is derived from (13) as

$$I_{pd} = (1 - 2D)I_0. \tag{15}$$

The peak-to-peak value ΔI_p of the current $i_{pa}(t)$ is given by

$$\Delta I_p = \frac{1}{L_p}\int_0^{DT} (E - E_c)\, dt = \frac{D(1 - D)TE}{L_p}. \tag{16}$$

Therefore, $i_p(t_0)$ and $i_p(t_3)$ are, respectively, derived below

$$i_p(t_0) = I_{pd} + \frac{\Delta I_p}{2} \tag{17}$$

$$i_p(t_3) = I_{pd} + \frac{\Delta I_p}{2}. \tag{18}$$

Substituting (17) and (18) into (7) and (8), $t_{\gamma a}$ and $t_{\gamma b}$ are given as

$$t_{\gamma a} = \frac{2CE}{2(1 - D)I_0 + (\Delta I_p/2)} \tag{19}$$

$$t_{\gamma b} = \frac{2CE}{2DI_0 + (\Delta I_p/2)}. \tag{20}$$

Because the saturable reactors are to block the load current during the switching transition intervals, the zero-voltage soft-commutation from S_1 to D_2, and from S_2 to D_1 can be achieved by the load current I_0. In case of no saturable reactors, $t_{\gamma a}$ and $t_{\gamma b}$ are given as

$$t_{\gamma a} = \frac{2CE}{-2DI_0 + (\Delta I_p/2)} \tag{21}$$

$$t_{\gamma b} = \frac{2CE}{-2(1 - D)I_0 + (\Delta I_p/2)}. \tag{22}$$

From (21) and (22), to maintain the zero-voltage soft-commutation, the current $(\Delta i_p/2)$ must be conditioned as $>2DI_0$ and $>2(1 - D)I_0$.

In comparison with (19)–(22), it is noted that the magnitude of $(\Delta I_p/2)$ can be substantially reduced by using each saturable reactor in series with the rectifier diode D_3 or D_4.

The voltage and current peak stresses for the active switches S_1 and S_2 are derived as follows:

$$V_{S1p} - E \tag{23}$$

$$V_{S1p} = I_0 + i_p(t_0) = 2(1 - D)I_0 + (\Delta I_p/2) \tag{24}$$

$$V_{S2p} = E \tag{25}$$

$$I_{S2p} = -\{-I_0 + i_p(t_3)\} = 2DI_0 + (\Delta I_p/2). \tag{26}$$

The output voltage E_0 is calculated by

$$E_0 = 2D(1 - D)E - (\hat{V}_{SL1} + \hat{V}_{SL2}) \tag{27}$$

where $\hat{V}_{SL1}$ and $\hat{V}_{SL2}$ are average voltages of SL_1 and SL_2,, respectively. The currents I_{pd}, I_{s1p}, and I_{s2p} depend on the

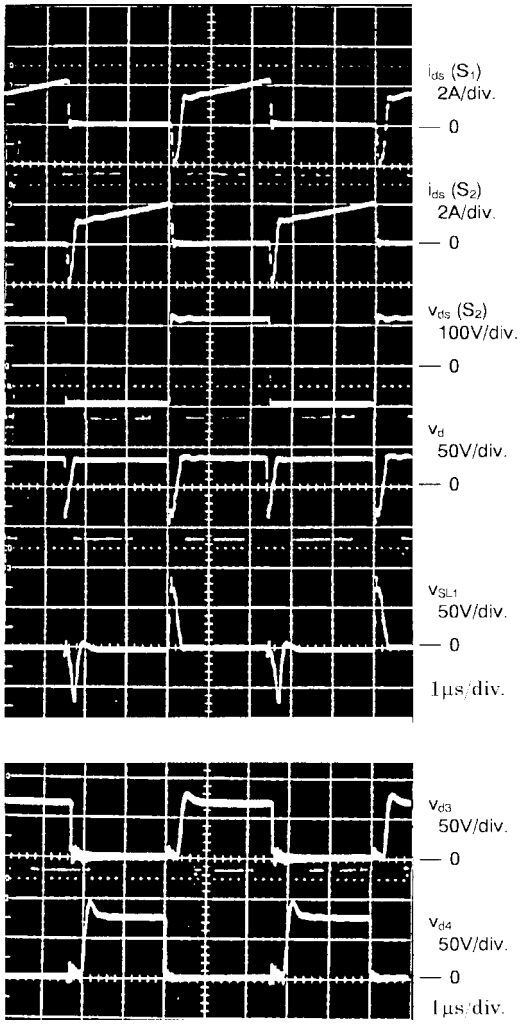

Fig. 3. Observed waveforms of converter ($E = 220$ V, $E_0 = 300$ V, $I_0 - 5$A).

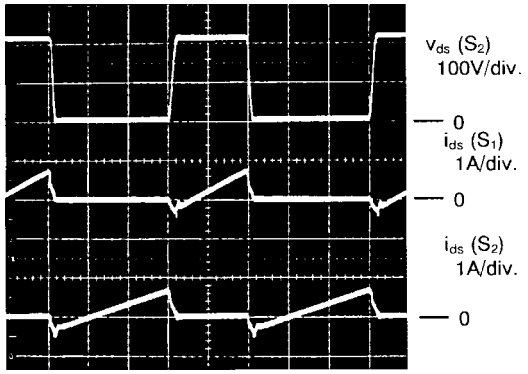

Fig. 4. Observed waveforms of converter with saturable reactors ($E = 220$ V, $E_0 = 30$ V, $I_0 = 0.5$A).

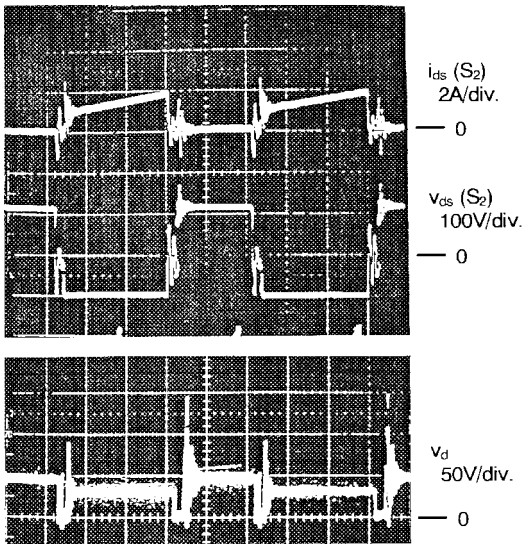

Fig. 5. Observed waveforms of converter without saturable reactors.

duty ratio D as a control variable D indicated below

$$\begin{cases} I_{pd} > 0 \\ I_{S1p} > I_{S2p} \end{cases} \quad \text{for } 0 < D < 0.5$$
$$\begin{cases} I_{pd} = 0 \\ I_{S1p} = I_{S2p} \end{cases} \quad \text{for } D = 0.5 \quad .$$
$$\begin{cases} I_{pd} < 0 \\ I_{S1p} < I_{S2p} \end{cases} \quad \text{for } 0.5 < D < 1$$

It can be considered that this power converter acts as a forward–flyback hybrid transformer operation. In this case, a maximum conversion ratio can be obtained in the case of the duty ratio $D = 0.5$. Thus, in order to regulate the average output voltage, the duty ratio D as a control variable should be selected within either $0 \leq D \leq 0.5$ or $0.5 \leq D \leq 1$.

III. Experimental Results

A. Experimental Set-Up

To verify the analytical results of this converter circuit, 150 W ($E_0 - 30$ V, $I_0 - 5$ A)–200-kHz prototype power converter is built and implemented for distributed telecommunication power supply. The design parameters of this converter circuit are:

S_1, S_2	Power MOSFET's ($V_{DSS} = 450$ V; $I_D = 12$ A);
C_1, C_2	250 pF;
C_3	4.7 μF;
Lp	227 μH;

Transformer winding ratio 3:1:1;
Saturation flux values of SL_1 or S_{L2}15 V·μs.

The additional inductor L_p is effectively substituted by the magnetizing inductance of the forward–flyback transformer incorporated into the intermediate power stage. Because the current $i_p(t)$ contains a dc component I_{pd}, the high-frequency transformer with EI type ferrite core is designed so as to realize a little air gap.

B. Observed Waveforms and Performances

Figs. 3 and 4 show the voltage and current waveforms of this power converter which are measured for full load and minimum load conditions at $E = 220$ V. As can be seen, this zero-voltage transition soft-switching technique based upon the operating principle of saturable reactor-assisted loss

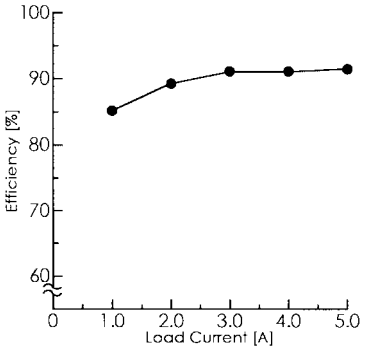

Fig. 6. Measured overall efficiency of converter.

capacitor snubber is completely maintained from full load to minimum load.

The voltage ringing and overshoot from the rectifiers are substantially reduced without extra complicated snubbers. In addition to this, the ripple factor of the rectified voltage $v_d(t)$ is also lowered effectively. Furthermore, The voltage–ampere (VA) ratings for the output low-pass filter can be considerably reduced as compared with that of half-wave rectified converter. For the full load, the duty ratio D as a control variable is set to $D = 0.48$.

Fig. 5 illustrates the observed voltage and current waveforms of the conventional high-frequency linked DC–DC power converter without the saturable reactors connected in series with each rectifier diode. As can be seen, the excessive voltage ringing and overshoot will apply to the power active switches and the power passive switches.

It indicates that the saturable reactors play an important role for achieving the complete zero voltage soft-switching. Fig. 6 shows the measured overall efficiency as a function of the load current. In this case, the power conversion efficiency of this power converter is 91.5% under full load condition and 90% under half load condition.

IV. Conclusions

A novel prototype topology of the zero voltage soft-switching transition asymmetrical PWM DC–DC converter with a high-frequency center-tapped forward & flyback transformer link using the saturable reactor and lossless capacitor-assisted soft-switching technique has been proposed as an improved version of hard switching PWM as well as resonant mode DC–DC converters. The principle of this converter operation are illustrated together with the circuit analysis in a steady-state. The characteristic performances of this converter using power MOSFET's are actually confirmed by a 150-W–200-kHz breadboard set-up. The substantial effectiveness of simple, economic, compact, saturable reactors composed of amorphous cores in the converter have also been proved and discussed from an experimental point of view. This saturable reactor-assisted SEPP ZVS-PWM DC–DC power converter with a high-frequency link includes the following advantages:

- low voltage stresses for the main switches and rectifier diodes;
- small ripple for the rectified voltage;
- lowered VA ratings of the saturable reactors used;
- reduced EMI;
- wide ZVS range from light to heavy loads;
- efficient operation;
- large current capability of low voltage output.

In the future, the transient performance analysis of the advanced soft-switching PWM DC–DC converter circuit treated here should be proceeded from an application point of view. In addition, the soft-switched power converter using the new generation trench-type MOSFET IGBT's should be investigated and evaluated from a practical point of view.

References

[1] O. D. Patterson and D. M. Divan, "Pseudo-resonant full bridge DC–DC converter," in *IEEE-PELS Power Electronics Specialists Conf. (PESC) Rec.*, June 1987, pp. 424–430.

[2] S. Hamada, Y. Ogino, and M. Nakaoka, "A 350 W–500 kHz PWM DC-DC converter utilizing saturable reactor assisted soft-switching technique," in *Proc. European Conf. on Power Electronics and Applications (EPE)*, Sept. 1991, pp. 1-538/1-543.

[3] S. Hamada and M. Nakaoka, "Family of saturable rector assisted soft-switching DC-DC converters," *Proc. Inst. Elect. Eng.*, Pt. B, vol. 139, no. 4, pp. 395–401, July 1992.

[4] S. Hamada, M. Michihira, anbd M. Nakaoka, "Using a tapped inductor for reducing conduction losses in a soft-switching PWM DC–DC converter," in *Proc. European Conf. on Power Electronics and Applications (EPE)*, Sept. 1993, pp. 130–134.

[5] S. Hamada and M. Nakaoka, "A novel saturable reactor assisted asymmetrical PWM forward-flyback hybrid DC–DC converter," in *Proc. Int. Conf. on Power Electronics*, Oct. 1995, pp. 349–354.

Junming Sun received the B.S. and M.S. degrees in electrical engineering from Tianjin University, Tianjin, China in 1985 and 1988, respectively. In 1996, as a Ph.D candidate student, he joined the graduate school of engineering and science of Yamaguchi University, Yamaguchi, Japan.

His current research interests include high-frequency resonant converters/inverters and digital control of power electronic converter applications.

Mr. Sun is a member of the Institute of Electrical Engineers of Japan.

Satoshi Hamada received the B.S. degree in electrical engineering from Osaka Institute of Technology, Osaka, Japan, in 1970. He received the Ph.D degree in electrical systems engineering from the graduate school of engineering and science, Yamaguchi University, Yamaguchi, Japan.

Dr. Hamada is a member of the Institute of Electrical Engineers of Japan, the Institute of Electronics, Information, and Communication Engineers of Japan.

Junji Yoshitsugu received the B.S. degree in electrical and electronic engineering from Yamaguchi University, Yamaguchi, Japan, in 1997. He is currently studying for the M.S. degree at the graduate school of engineering and science, Yamaguchi University, Yamaguchi, Japan.

His research interests include power electronic converter control and motion control drive application.

Mr. Yoshitsugu is a member of the Institute of Electrical Engineers of Japan.

Bin Guo received the B.S. degree in electrical engineering and computer science from Shanghai Jiao-Tong University, China, in 1987 and the M.S. degree in electrical engineering from Kobe University of Mercantile Marine, Japan, in 1995. He has been working toward the Ph.D. degree at the Graduate School of Engineering and Science, Yamaguchi University, Japan.

His current research interests include high-frequency induction heated inverters..

Mr. Guo is a member of the Institute of Electrical Engineers of Japan and the Marine Engineering Society in Japan.

Mutsuo Nakaoka (M'83) received the Ph.D. degree in electrical engineering from Osaka University, Japan in 1981.

He has been a Professor in the electrical and electronics engineering department of Kobe University, Japan. Since 1995, he has been a professor in electrical and electronics engineering, the graduate school of engineering and science, Yamaguchi University, Yamaguchi, Japan. His research interests include advanced developments on the state-of-art power electronic circuits and systems engineering.

Dr. Nakaoka is a member of the Institute of Electrical Engineers of Japan, Japan Society of Power Electronics, the Society of Instrument and Control Engineers, the Institute of Systems, Control and Information of Japan, and the Institute of Electronics, Information, and Communication Engineers of Japan.